



**Head-on collision of compressional shocks in two-dimensional Yukawa systems**Xia Ding,<sup>1</sup> Shaoyu Lu,<sup>1</sup> Tianyue Sun,<sup>1</sup> M. S. Murillo <sup>2</sup> and Yan Feng <sup>1,\*</sup><sup>1</sup>*Center for Soft Condensed Matter Physics and Interdisciplinary Research, School of Physical Science and Technology, Soochow University, Suzhou 215006, China*<sup>2</sup>*Department of Computational Mathematics, Science and Engineering, Michigan State University, East Lansing, Michigan 48824, USA*

(Received 8 March 2020; revised 19 November 2020; accepted 1 December 2020; published 7 January 2021)

The head-on collision of compressional shocks in two-dimensional dusty plasmas is investigated using both molecular dynamical and Langevin simulations. Two compressional shocks are generated from the inward compressional boundaries in simulations. It is found that, during the collision of shocks, there is a generally existing time delay of shocks  $\tau$ , which diminishes monotonically with the increasing compressional speed of boundaries, corresponding to the time resolution of the studied system. Dispersive shock waves (DSWs) are generated around the shock front for some conditions. It is also found that the period of the DSW decreases monotonically with the inward compressional speed of boundaries, more substantially than the time delay of shocks  $\tau$ . When the inward compressional speed of boundaries increases further, the DSWs gradually vanish. We speculate that, for these high compressional speeds of boundaries, the period of the DSW might be reduced to a comparable timescale of the time delay of shocks  $\tau$ , i.e., the time resolution of our studied system, or even shorter, thus the DSW reasonably vanishes.

DOI: [10.1103/PhysRevE.103.013202](https://doi.org/10.1103/PhysRevE.103.013202)**I. INTRODUCTION**

A dispersive shock wave (DSW) is a periodic structure generated after the breaking of a powerful pulse in a wave system where the dispersive effect is much larger than the dissipative one [1]. For example, a tidal bore observed in water [2] is one typical example of a DSW. In addition to this tidal bore, a DSW has also been found in the Bose-Einstein condensates [3,4], the nonlinear optics [5,6], and dusty plasmas [7].

Dusty plasma, or complex plasma, is an experimental model system in which the motion of individual dust particles can be directly studied at the kinetic level using the diagnostic of the video imaging [8–16], so that quite a few physical processes, like shocks [17], can be investigated in dusty plasmas at the kinetic level. In the laboratory conditions, these dust particles are strongly coupled [18,19] due to their high negative charges [20,21], and a single-layer suspension of dust particles can be formed in the plasma sheath, i.e., the two-dimensional (2D) dusty plasma. The interparticle interaction between these dust particles can be described as the Yukawa potential [19,22], although in some conditions the wake effect [23] of the ion flow may induce the nonreciprocal interaction [24] between dust particles. To mimic dusty plasmas, simulations of Yukawa systems [25–30] are often performed to investigate the collective dynamics of dusty plasmas. Quite a few fundamental physics processes have been studied intensely using the dusty plasma system, such as Refs. [31–36].

The wave interaction is a crucial problem in the study of dusty plasmas. Various related topics have been investigated, such as the collision of dust acoustic solitons [37], the

interference of two dust acoustic waves [38], soliton interaction [39], and so on. In the experimental and numerical investigations of the interaction of two counterpropagating solitons in Ref. [39], it is found that the solitons are delayed after the collision, and this delay time increases with the excitation amplitude. In the simulation of 2D Yukawa systems with an inward moving boundary, a compressional shock can be generated [7]. In Ref. [40], the shock Hugoniot curves after this compressional shock are analytically fitted under various conditions, so that different physical quantities after shocks are obtained from the derivation.

The DSW has been observed in the simulation of shocks in dusty plasmas [7] with some conditions of the specific values of the damping rate and Mach number. It is also found that [7], for some other conditions, the DSW structure cannot be observed anymore, called the vanishment of the DSW. However, the essential physics of DSWs in dusty plasmas is not yet understood. In this sense, we must explore the underlying physics of DSWs, as well as the relationship between DSWs and the collision of compressional shocks.

Here, we study the underlying physics of the head-on collision of two compressional shocks, as well as the generated DSW, in 2D dusty plasmas, using both frictionless molecular dynamics (MD) and Langevin simulations of Yukawa systems. Two pistons moving inward with a constant speed of  $v_p$  generate two compressional shocks with the inward propagating speed of  $D$  [40]. When the two shock waves continue to propagate away, they collide with each other, and later two new shock fronts are generated. In this process, a time interval between the two shock waves that collide and pass through can be observed; this is termed the time delay of shocks  $\tau$ . We find that this time delay of shocks diminishes monotonically with the increasing moving speed of two pistons. In Sec. II,

\*fengyan@suda.edu.cn

we briefly introduce our simulation methods. In Sec. III, we present three topics of the time delay of shocks, the period of the DSW, and the vanishment of the DSW, respectively. The DSW results presented here are well consistent with those in [7]. Moreover, from the many more data points presented here, we provide our physical explanation of the DSW vanishment in some conditions. Finally, we present our summary. Note that the results of the DSW in 2D Yukawa systems obtained here may also be applicable to other systems, such as, e.g., dense liquids [41].

## II. SIMULATION METHOD

To investigate the propagation of the head-on collision of two compressional shocks in 2D dusty plasmas, we perform frictionless MD simulations of 2D Yukawa systems using LAMMPS [42]. In our simulations,  $N = 16\,384$  simulated particles are constrained in a 2D plane, with the equation of motion [40,43] for each particle  $i$  of

$$m\ddot{\mathbf{r}}_i = -\nabla \sum_{j \neq i}^N \phi_{ij} + F_i^{\text{pis-left}} + F_i^{\text{pis-right}}. \quad (1)$$

Here, the first term is the interparticle interaction of the Yukawa potential of  $\phi_{ij} = Q^2 \exp(-r_{ij}/\lambda_D)/4\pi\epsilon_0 r_{ij}$ , where  $Q$  is the particle charge,  $r_{ij}$  is the distance between the particles  $i$  and  $j$ , and  $\lambda_D$  is the Debye length. The latter two terms on the right-hand side of Eq. (1) are both the confinement from the boundaries of the simulation box, as explained next. Note that here we would like to clarify that in dusty plasma experiments, the interparticle interaction may be much more complicated than the Yukawa repulsion; for example, the ion flow induced wake effect may result in the nonreciprocal interaction between these dust particles [23,24]. As in most simulation investigations, such as Ref. [7], here we also neglect the wake effect to use the Yukawa repulsion to describe the interparticle interaction for 2D dusty plasmas, so that the results here are mainly for the physics of 2D Yukawa systems.

In our simulations, two compressional shocks are generated from the two inward moving boundaries to mimic two pistons. To simulate the force from the left-hand-side piston, we use the form of a Gaussian function  $\vec{F}_i^{\text{pis-left}} = 50 \exp(-(x - x_p^l)^2/0.25a_0^2) m a_0 \omega_{pd}^2 \hat{x}$  acting on all simulated particles, where  $x_p^l$  is the location of the piston in the  $x$  direction moving with a constant speed  $v_p$ . The function of the force from the right-hand-side piston is similar, with the other piston in the symmetric location  $x_p^r$  moving in the reverse direction. During our simulations, two pistons move inward at a constant speed  $v_p$  at the same time, and we record the positions and velocities of simulated particles for the later data analysis. In our simulation, the inward compressional speed of two boundaries is chosen from  $0.141 a\omega_{pd}$  to  $1.272 a\omega_{pd}$ , so that the corresponding Mach number of the inward compressional speed  $M_p = v_p/C_l$  varies from 0.147 to 1.324. At the same time, the shock front, generated by the moving pistons, can be easily observed in Fig. 1. The corresponding shock front speed  $D$  can be determined from the slope of the boundary between the compressed and uncompressed regions in the spatiotemporal evolution of the number density for particles  $n$ , as we will describe later.

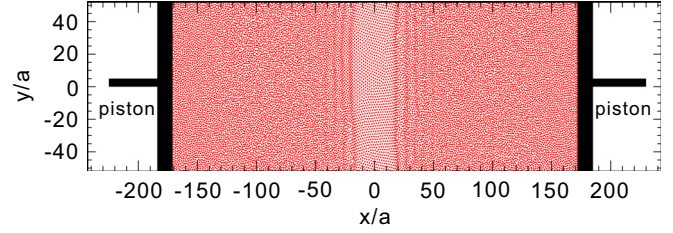


FIG. 1. Snapshot of particle positions of two-dimensional Yukawa solids before the head-on collision of two compressional shocks in our simulations. Two pistons on the left and right boundaries both move inward with a constant speed of  $v_p$ , generating two compressional shocks with the inward propagating speed of  $D$  [40]. At the shock front region, a few ripples of the particle density appear, called the dispersive shock wave (DSW). Here, we focus on the properties of the DSW and the dynamics of the latter head-on collisions of these two compressional shocks. Note that, in our simulations ( $N = 16\,384$ ) reported here, the periodic boundary conditions are applied in the  $y$  direction.

Here are some details in our simulations. In the  $y$  directions, we use the periodic boundary conditions as in [40,43]. We choose the initial conditions of our simulated 2D Yukawa system to be  $\Gamma = 800$  and  $\kappa = 0.75$ , for example. Before generating shocks, we perform our MD simulation  $> 2 \times 10^5$  steps to make sure that the simulated system reaches the steady state of  $\Gamma = 800$  and  $\kappa = 0.75$ . Then we apply two moving boundaries in the  $x$  direction to generate shocks to record the data for the investigations reported here. Besides the initial conditions of  $\Gamma = 800$  and  $\kappa = 0.75$ , we also perform other simulation runs with the different coupling parameter of  $\Gamma = 200$  and the various screening parameters of  $\kappa = 1.0$  and  $2.0$ . Note that, for each simulation run, the Debye length  $\lambda_D$  is unchanged. As a result, when the pistons move inward to compress the system, the value of  $\kappa$  decreases, as in [40].

In dusty plasma experiments, the motion of dust particles is underdamped [19] due to the frictional gas drag acting on these dust particles while they move. To study the effects of gas damping on the DSW, we also perform Langevin dynamical simulations [44] to mimic the propagation of the head-on collision of two compressional shocks in 2D dusty plasma experiments. The equation of motion of each particle is similar to Eq. (1), except that we add two more terms on the right-hand side. The first term  $\nu m \dot{\mathbf{r}}_i$  is the Epstein frictional gas drag expression [45], where  $\nu$  is the gas damping rate. The second term is the Langevin random kicks from the fluctuation-dissipation theorem [45]. In our simulations, we specify the gas damping rate as  $\nu/\omega_{pd} = 0.037$ , comparable to the typical dusty plasma experiments [20], while other parameters are exactly the same as those in the MD simulations above. Other details of our Langevin simulations are similar to [44,45].

## III. RESULTS AND DISCUSSIONS

### A. The time delay of shocks $\tau$

To determine the time delay of shocks  $\tau$ , we prepare a spatiotemporal evolution of the number density  $n$  of particles

for the head-on collision of two compressional shocks, as in Fig. 2. First, we divide the simulation region into 480 rectangular bins with the width of  $a$  in the  $x$  direction, and we count the number of particles in each bin, called the number density  $n$ . Then we plot the counted number as a function of the time  $t$  and the position  $x$ , as in Fig. 2(a), which is just the spatiotemporal evolution of the number density  $n$  of particles.

From Fig. 2, as well as the spatiotemporal evolution of the number density  $n$  for other compressional speeds, we find that the time delay of shocks  $\tau$  generally exists for our studied 2D Yukawa systems with all different compressional speeds. The shock front is at the border between the disturbed and undisturbed regions, thus the slope of this border in Fig. 2, as those dashed lines show there, is just the shock front speed  $D$  [40]. After the collision, two new shock fronts are generated, marked as the dotted lines. Clearly, there is a time delay of  $\tau\omega_{pd} = 2.5$  in Fig. 2(b) before two new shocks propagate away at the conditions of  $\Gamma = 800$ ,  $\kappa = 0.75$ , and  $M_p = 0.441$ . As the substance or media for the propagation of shocks and waves, individual particle motion of the 2D Yukawa system has its own timescale. For the condition of  $M_p = 0.441$  in Fig. 2, the observed time delay of shocks  $\tau\omega_{pd} = 2.5$  can also be expressed as  $\tau\omega_E < 2.5$  using the Einstein frequency [27], which is less than half of the vibration period for individual particles. We speculate that this time delay of shocks may be related to the timescale of the individual particle motion. In principle, for small disturbance, this time should not be shorter than  $1/4$  of the vibration period of individual particles, i.e.,  $t \gtrsim 2\pi\omega_{pd}^{-1}/4$ . However, for stronger shocks, particles around the shock front are accelerated further, so that this time delay can be shortened. Next, we present the measured time delay for different inward compressional speeds of  $M_p$  in Fig. 3.

From Fig. 3, we find that the time delay of shocks  $\tau$  diminishes monotonically with the increasing Mach number of the compressional speed of boundary  $M_p$ . When the compressional speed of boundary increases, the generated shock is more extreme, so that particles move faster. As a result, the time delay of shocks  $\tau$  becomes shorter. When the time delay of shocks  $\tau$  drops to the level of  $\tau\omega_{pd} \approx 1$ , it seems that this time delay cannot drop substantially further even though  $M_p$  increases. Besides the MD simulations for the conditions of  $\Gamma = 800$  and  $\kappa = 0.75$  presented in Fig. 3, we also perform quite a few other simulation runs with different values of  $\Gamma$  and  $\kappa$ . It seems that the obtained time delay of shocks  $\tau$  is not related to the values of  $\Gamma$  and  $\kappa$ , as presented in detail in [46]. Thus, we conclude that the time scale of  $\tau\omega_{pd} \approx 1$  is just the time resolution of our studied systems, which should be related to the timescale of the individual particle motion, leading to the property of the DSW.

Note that a few stripes around the shock front in Fig. 2 reflect the structure of the DSW. Later, after the head-on collision of two shocks, these stripes form a grid, as shown in Fig. 2, corresponding to the interaction of DSW. Also, the observed shock front speed after the collision  $D'$  in Fig. 2 is slightly smaller than the shock front speed  $D$  before the collision. Before the collision of two shocks, in the after-shock region, the studied 2D Yukawa system has a higher

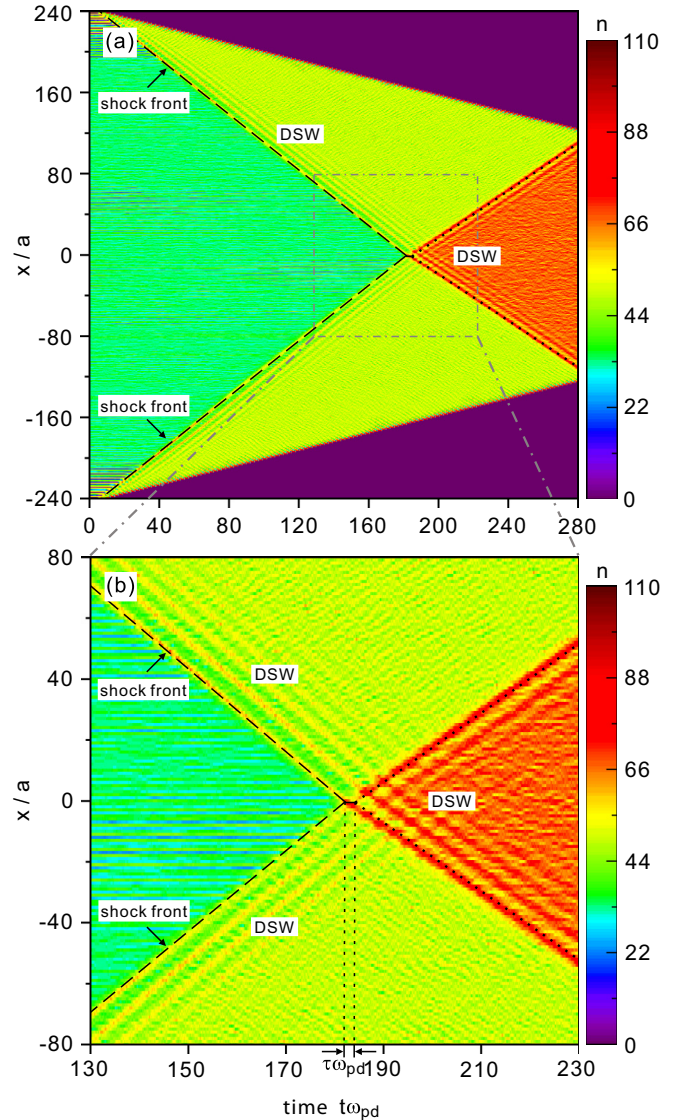


FIG. 2. The spatiotemporal evolution of the number density  $n$  of particles for the head-on collision of two compressional shocks when  $M_p = 0.441$  for the 2D Yukawa conditions of  $\Gamma = 800$  and  $\kappa = 0.75$ . The simulation box is divided into 480 narrow rectangular bins with the width of  $a$  in the  $x$  direction, and the counted particle number in each bin is just the plotted number density here. Two shock fronts can clearly be observed from this number density evolution in (a) as two distinctive lines with the constant slope, corresponding to the shock front speed  $D$ , which we marked as the dashed line. These two distinctive lines merge together when  $t\omega_{pd} = 181$ , which means that these two shock fronts collide with each other. By magnifying the collision procedure in (a), as in (b), we can see that, after the head-on collision of these two shock fronts (marked as the dashed line), there is a clear time delay of  $\tau\omega_{pd} = 2.5$  before two new shocks (marked as the dotted line) propagate away. The variation property of this time delay of shocks  $\tau$  as a function of the Yukawa conditions and the shock parameters is what we will study here. Note that, in both panels, before the head-on collision of two shocks, we observe a few stripes with the same slope of the shock front, reflecting the structure of the DSW. Also, after the collision, these stripes form a grid, further reflecting the interaction of the DSW.

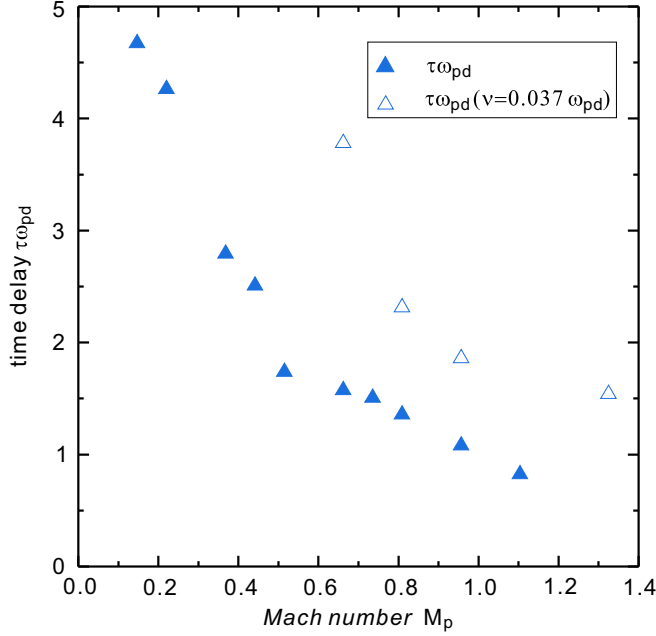


FIG. 3. The time delay of shocks  $\tau$  as the function of the Mach number of the inward compressional speed  $M_p$  for the 2D Yukawa conditions of  $\Gamma = 800$  and  $\kappa = 0.75$ . We obtain the time delay of shocks  $\tau$  in different Mach numbers with and without frictional gas drag from the spatiotemporal evolution plots of the number density  $n$ , when the Mach number of the inward compressional speed  $M_p = v_p/C_l$  is varied from 0.147 to 1.324. Here, the time delay of shocks  $\tau$  decreases monotonically with the compressional speed of  $v_p$  for both conditions with and without frictional gas drag, and it seems to reach a saturation level of  $\tau\omega_{pd} \approx 1$  at the high Mach numbers from our simulation. We speculate that the observed timescale of  $\tau\omega_{pd} \approx 1$  is related to the timescale of individual particle motion.

kinetic temperature of  $\Gamma = 38$  and a lower screening parameter of  $\kappa = 0.62$ , where the later generated shocks after the collision propagate. Under these conditions, using our simulations not reported here, we obtain the corresponding shock Hugoniot curve, or the  $D - \bar{v}$  relationship, as  $D = 1.081 + 0.896\bar{v} + 0.116\bar{v}^2$ , using the method in [40]. The particles around the region where the later generated shock propagates ( $t\omega_{pd} > 180$ ) should have the overall drift motion in the reversed direction, and we calculate this drift velocity of  $\bar{v} = 0.425a\omega_{pd}$  from our simulation data reported here. Substituting the obtained  $\bar{v} = 0.425a\omega_{pd}$  into the shock Hugoniot curve above, we can predict the shock front speed of  $1.483a\omega_{pd}$  under these conditions. From the dotted lines shown Fig. 2, we can directly measure shock front speed after the collision, which is  $D' = 1.163a\omega_{pd}$ . We find that this measured shock front speed  $D' = 1.163a\omega_{pd}$  is almost equal to  $1.483a\omega_{pd} - 0.425a\omega_{pd} = 1.058a\omega_{pd}$ , i.e., the predicted shock front speed of  $1.483a\omega_{pd}$  from the system without a drift motion subtracted by the obtained drift velocity  $\bar{v}$  from our studied shock collision system here, with only less than 10% uncertainty from our data analysis.

In addition to the results from our frictionless MD simulations above, we also plot our obtained results of the time delay of shocks from our Langevin simulations in Fig. 3, as shown by the hollow symbols. Clearly, for each inward compressional

speed  $v_p$ , the time delay of shock  $\tau$  from the Langevin simulation is always larger than that from the frictionless MD simulation. We also find that the time delay of shocks  $\tau$  diminishes monotonically with the increasing compressional speed of boundary  $v_p$ . Clearly, although the frictional gas damping expands the time delay of shocks  $\tau$ , the variation trend of  $\tau$  as a function of  $v_p$  is unchanged.

The time delay of the head-on collision of solitons has been experimentally observed in [39], which in principle should be similar to our observation of the time delay of shocks  $\tau$  here. In [39], the observed time delay  $1.108 \omega_{pd}^{-1}$  is consistent with our obtained time delay of shocks  $\tau\omega_{pd} \approx 1$  for the conditions of higher Mach numbers. Meanwhile, there are some differences between the experiment results [39] and our simulations. For example, in [39] it is found that the time delay increases with the amplitude of solitons; however, in our two types of simulations, this time delay is always diminished substantially and monotonically when the inward compressional speed increases, or when the amplitude increases.

## B. The period of DSW

To investigate the period of the DSW, in Fig. 4 we compute the one-particle distribution function  $f_1(\zeta, v_x)$ , as in [7]. Here,  $\zeta$  is the Lagrange coordinate  $\zeta = (x - Dt)$ , which is the moving coordinate with the generated DSW. First, we calculate the shock front speed  $D$  at different inward compressional speeds of two boundaries from the spatiotemporal evolution of particles, which varies from  $1.113 a\omega_{pd}$  to  $2.322 a\omega_{pd}$  for different runs in our simulation data. Then we count the particle number in different coordinates of  $\zeta$  and  $v_x$ . We divide the horizontal axis of  $\zeta$  into bins with a width of  $0.5a$ , and we divide the vertical axis of  $v_x$  into bins with a width of  $0.005 a\omega_{pd}$ . Then, we count the particle number of each cell and divide it by the total particle number in all cells to obtain the one-particle distribution function  $f_1(\zeta, v_x)$ . Here we present six typical results, with the corresponding piston Mach numbers of 0.22, 0.441, 0.662, 0.809, 0.956, and 1.324, as shown from Figs. 3(a)–3(f).

The wavelength and period of the DSW can be directly measured from the obtained  $f_1(\zeta, v_x)$ . As shown in Fig. 4(a), we mark the location of the first three peaks of  $f_1(\zeta, v_x)$ . Then the measured distance between the first and second peaks is just the first wavelength, marked as  $\lambda_1$ . Similarly, the distance between the second and third peaks is the second wavelength, marked as  $\lambda_2$ . Note that, from our calculated one-particle distribution function  $f_1(\zeta, v_x)$ , the most prominent feature is that the wavelengths of  $\lambda_1$  and  $\lambda_2$  both decrease monotonically with the increasing compressional speed of the two boundaries. We also calculate the period of the DSW using  $T = \lambda/D$ , where  $D$  is the shock front speed, so that  $T_1$  and  $T_2$  are the first and second periods of the DSW.

Interestingly, when the Mach number increases, it becomes more and more difficult to distinguish the wavelength from  $f_1(\zeta, v_x)$ . From Figs. 4(a)–4(f), when the inward compressional speed of two boundaries  $v_p$  is larger, the generated DSW has a larger amplitude and a smaller wavelength. Furthermore, an increasing compressional speed of two boundaries  $v_p$  gradually blurs the feature of the DSW in  $f_1(\zeta, v_x)$  until it vanishes almost completely in Fig. 4(f). We

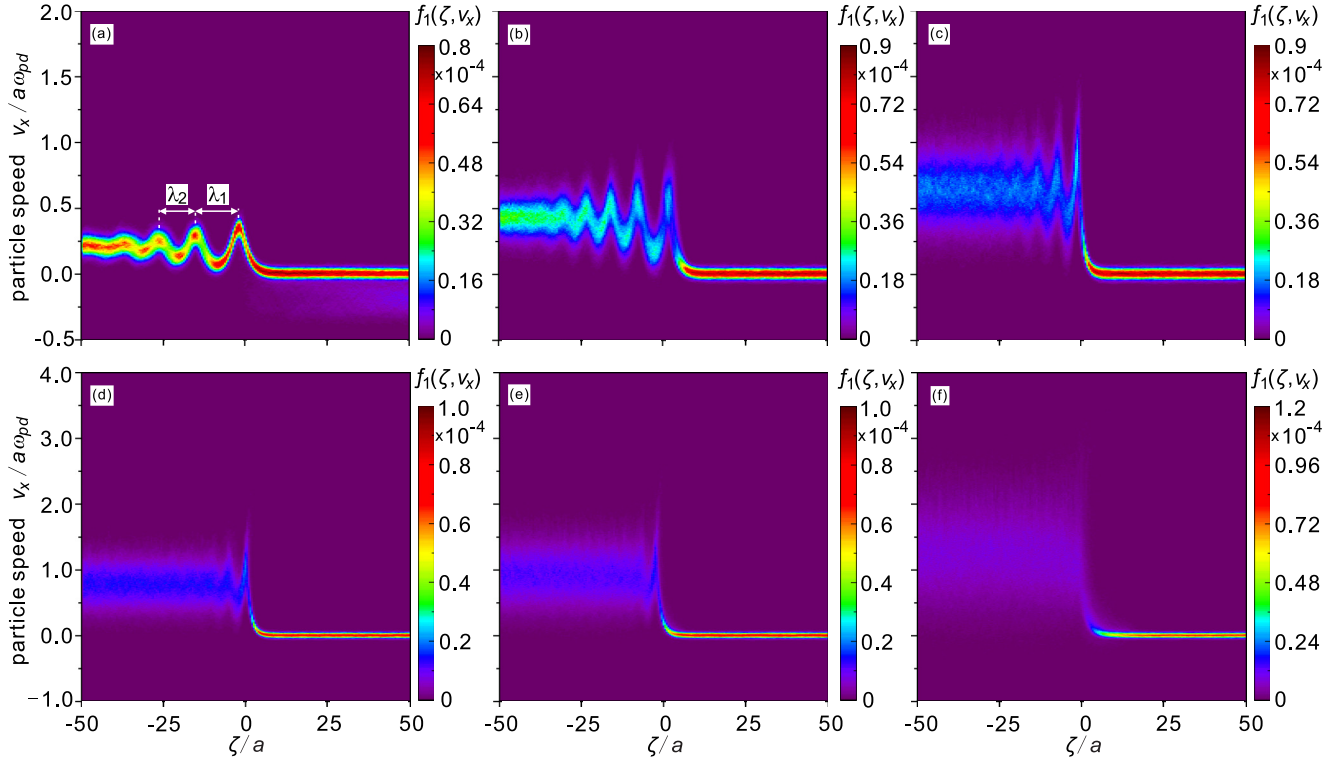


FIG. 4. The obtained one-particle distribution function  $f_1(\zeta, v_x)$ , where  $\zeta$  is the Lagrange coordinate  $\zeta = (x - Dt)$ , from our frictionless MD simulations of  $\Gamma = 800$  and  $\kappa = 0.75$ . To calculate  $f_1(\zeta, v_x)$ , we divide the  $\zeta$ - $v_x$  plane into bins in both the  $\zeta$  and  $v_x$  directions, and we count the particle number in each cell. Then, we divide the counted number in each cell by the total particle number in all cells to obtain the one-particle distribution function  $f_1(\zeta, v_x)$ , as in [7]. In our simulations, the only varied condition is the inward compressional speed of two boundaries in the  $x$  direction, which are (a)  $M_p = 0.22$ , (b)  $M_p = 0.441$ , (c)  $M_p = 0.662$ , (d)  $M_p = 0.809$ , (e)  $M_p = 0.956$ , and (f)  $M_p = 1.324$ , respectively. Here, we refer to the distance between the first and second peaks of  $f_1(\zeta, v_x)$  in the shock front as the first wavelength of the oscillation  $\lambda_1$ . Similarly, the distance between the second and third peaks is called the second wavelength  $\lambda_2$ , as marked in (a). Clearly, from (a)–(f), the wavelengths  $\lambda_1$  and  $\lambda_2$  gradually diminish with the Mach number, until the DSW completely vanishes. Note that we also find that the first wavelength  $\lambda_1$  seems to be always slightly larger than the second one  $\lambda_2$ .

speculate that a larger compressional speed of two boundaries  $v_p$  would generate more severe shocks containing more kinetic energy, so that the structure of the DSW would be damaged more by these active particles.

The velocity distribution in the postshock region varies a lot when the compressional speed of the boundaries changes. In Fig. 4(a), the velocity distribution is pretty narrow. Then, as the boundary speed increases, the velocity distribution in the postshock region increases monotonically. When the compressional speed of the boundary is higher, the particles in the simulated system are more severely disturbed, so that more energy from the compression is converted to the thermal energy, i.e., the velocity distribution is wider. We also speculate that, since the kinetic temperature of particles is higher for a faster compressional speed of boundaries, this higher temperature may also blur the DSW until it gradually vanishes.

Note, the DSW results presented in Fig. 4 are the averaging of all frames in the steady state. In [46], we also provide the evolution of the DSW in our simulations, from the initial compression of the boundary to the final steady state when the DSW is fully developed. For each snapshot of the DSW, we also create the Fourier transformation of the number density ripples in order to find the evolution of the corresponding

wave-number peak location, which may be useful in the construction of the DSW theory in the future.

### C. Vanishment of the DSW

To explore the physical mechanism of the vanishment of the DSW, we investigate the variation of the period of the DSW as a function of the inward compressional speed of the boundary. For the different compressional speeds of boundaries, we obtain the first and second periods ( $T_1$  and  $T_2$ ) of the DSW using  $T = \lambda/D$ , where the wavelengths of  $\lambda_1$  and  $\lambda_2$  are directly measured from the calculated  $f_1(\zeta, v_x)$  in Fig. 4. For some high compressional speeds, the DSWs fade away so that the period cannot be distinguished anymore, which we just ignore.

As the major result of this paper, our obtained periods of the DSW are presented with the time delay of shocks in Fig. 5. We find that both the first and second periods of the DSW decrease monotonically with the compressional speed  $v_p$ . The first and second periods ( $T_1$  and  $T_2$ ) of the DSW are both always larger than the time delay of shock  $\tau$ , although  $T_1$  and  $T_2$  decrease much more substantially than  $\tau$  when  $M_p$  increases. In addition to the results of  $T_1$  for the conditions of  $\Gamma = 800$  and  $\kappa = 0.75$  presented in Fig. 5, the results of the

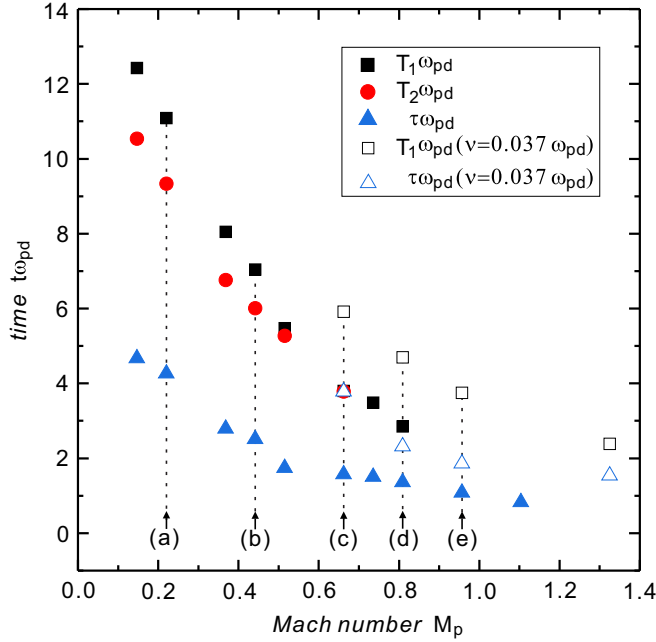


FIG. 5. The time delay of shocks  $\tau$  (triangle), and the first  $T_1$  (square) and second  $T_2$  (circle) periods of the DSW, as functions of the inward compressional speed of boundary  $v_p$  for the 2D Yukawa conditions of  $\Gamma = 800$  and  $\kappa = 0.75$ . Here, the time delay  $\tau$  is obtained from Fig. 3, while the first and second periods  $T_1$  and  $T_2$  of shock waves are obtained from  $T = \lambda/D$ , where  $\lambda_1$  and  $\lambda_2$  are measured from the calculated  $f_1(\zeta, v_x)$  as in Fig. 4. When the compressional speed of the boundaries  $v_p$  increases, the three timescales (the time delay of shocks  $\tau$ , and the first  $T_1$  and second  $T_2$  periods of dispersive shock waves) all decrease monotonically. We can find that the first and second periods  $T_1$  and  $T_2$  of shock waves are always larger than the time delay of shock  $\tau$ , although  $T_1$  and  $T_2$  diminish much more substantially than  $\tau$ . And the time delay of shocks  $\tau$  seems to reach a saturation level of  $\tau\omega_{pd} \approx 1$  at the high Mach numbers from our simulation data. We speculate that the unity timescale of  $\tau\omega_{pd} \approx 1$  seems to be related to the motion of individual particles around the shock front. We believe that the observed timescale of  $\tau\omega_{pd} \approx 1$  is just the time resolution of our studied shock system, which determines the property of the DSW. We speculate that, for a high Mach number of  $v_p$ , the period of the DSW might be reduced to the time resolution of our studied system, or even shorter. As a result, the DSW cannot be detected anymore with this time resolution, and the DSW reasonably vanishes around the shock front. Note that the legends of (a)–(e) correspond here to the results of the panels in Fig. 4. We also plot the results of the obtained time delay of shocks and the first period of shock wave from the Langevin simulations, as two types of hollow symbols shown. Clearly, although the frictional gas damping expands both the time delay of shocks  $\tau$  and the first period of DSW  $T_1$ , the whole variation trends of  $\tau$  and  $T_1$  as a function of  $v_p$  are still the same as the case without gas damping.

period of the DSW for other conditions with different values of  $\Gamma$  and  $\kappa$  are presented in detail in [46]. From [46], the period of the DSW is not affected much by the values of  $\Gamma$  and  $\kappa$ . For various conditions of 2D Yukawa systems, it seems that the period of the DSW is almost a function of only one

variable  $M_p$ , the Mach number of the compressional speed of the boundary.

From Fig. 5 and [46], we can provide our explanation of the vanishment of the DSW from our simulation investigations. When the compressional speed of boundaries increases, both the period of the DSW and the time delay of shocks decrease monotonically. The period of the DSW decreases much more substantially than the time delay of shocks  $\tau$ . However, the time delay of shocks  $\tau$  can be regarded as the time resolution of the studied shock systems, which is probably related to the motion of individual particles around the shock front as we speculate. The DSW is a kind of wave carrying the energy to propagate away. If the period of the DSW is comparable to or even smaller than the time delay of shocks  $\tau$ , then the DSW definitely vanishes, since the studied system (medium) cannot sustain such a small temporal resolution for the DSW anymore. We think, for the conditions of  $M_p > 0.8$  in Fig. 5, the undetectable periods of the DSW should be comparable to or even smaller than the time delay of shocks  $\tau$ , so that we cannot observe the DSW in the calculated one-particle distribution function  $f_1(\zeta, v_x)$  in those conditions anymore, such as in Fig. 4(f).

We also find that the first period of the DSW  $T_1$  is slightly larger than the second period  $T_2$ . We speculate that this is probably due to the temperature rise after the first wavelength has not reached the final steady value, as compared with the second wavelength. From Fig. 4, especially for the first three panels, velocity distribution in the first wavelength is narrower than that in the second wavelength and later. That is to say, after the propagation of the first wavelength, the 2D Yukawa system is not heated enough, while after the second wavelength propagation and even further, the 2D Yukawa system is heated enough, so that the kinetic temperature finally reaches the final steady state. From the main trend of Fig. 4, when the final temperature is higher, the corresponding wavelength is smaller. Thus, it is reasonable that  $T_1 > T_2$  since the studied system has not been heated enough during the propagation of the first wavelength of the DSW.

We also plot our obtained first period of the DSW  $T_1$  from our Langevin simulations in Fig. 5. Clearly, the first period of the DSW  $T_1$  is also expanded by the frictional gas drag, the same as the time delay of shocks  $\tau$ . However, the variation trend of  $T_1$ , as a function of  $v_p$ , is still unchanged. More importantly, when the first period of the DSW  $T_1$  is larger than the time delay of shocks  $\tau$ , the DSW can still be observed. This point obtained from the Langevin simulations is the same as that from the frictionless MD simulations. Of course, from Fig. 5, due to the effect of the frictional gas damping, the vanishment of the DSW probably happens at a larger Mach number of  $v_p$  as compared to the frictionless MD simulations. Further investigations related to the corresponding Langevin simulations are beyond the scope of this paper.

#### IV. SUMMARY

In summary, we systematically investigate the head-on collision of the compressional shocks in 2D Yukawa systems at the kinetic level, using frictionless MD and Langevin dynamical simulations of shocks generated from the inward compression of two boundaries.

From the spatiotemporal evolution of the number density  $n$  for different compressional speeds, we find that, after the collision of two shocks and before the generation of two new shocks, there is a time delay of shocks  $\tau$ . We obtain the value of this time delay of shocks  $\tau$ , which diminishes monotonically with the inward compressional speed of boundaries. It seems that, when the compressional speed of boundaries increases, the obtained time delay of shocks saturates around the level of  $\tau\omega_{pd} \approx 1$ , corresponding to the timescale of the motion of individual particles. We think that this time delay of shocks  $\tau$  probably corresponds to the time resolution of our studied 2D Yukawa systems, which determines the property of the DSW.

Using the one-particle distribution function  $f_1(\zeta, v_x)$ , we investigate the properties of the DSW. The first and second wavelengths and periods of the DSW are measured from the calculated  $f_1(\zeta, v_x)$  for some conditions. However, for other conditions, the DSW vanishes from the obtained  $f_1(\zeta, v_x)$ . We find that both the period of the DSW and the time delay of shocks decrease monotonically with the inward compressional speed, although the decrease of the period of the DSW is much more substantial. Our interpretation about the van-

ishment of DSW is that, when the period of the DSW is reduced to comparable to or even shorter than the time delay of shocks, i.e., the time resolution of our studied system, the DSW reasonably vanishes.

From the comparison between frictionless MD and Langevin simulations, we find that the frictional gas damping expands both the time delay of shocks  $\tau$  and the period of the DSW. However, the main variation trends of these two quantities, as the functions of the inward compressional speed of boundary  $v_p$ , are not changed. As a result, the frictional gas damping does not affect our conclusions obtained from the frictionless MD simulations above.

#### ACKNOWLEDGMENTS

Work in China was supported by the National Natural Science Foundation of China under Grant No. 11875199, the 1000 Youth Talents Plan, startup funds from Soochow University, and the Priority Academic Program Development (PAPD) of Jiangsu Higher Education Institutions. We thank the anonymous referees very much for providing constructive suggestions.

- 
- [1] Y. Matsuno, V. S. Shchesnovich, A. M. Kamchatnov, and R. A. Kraenkel, *Phys. Rev. E* **75**, 016307 (2007).
  - [2] S. Trillo, M. Klein, G. F. Clauss, and M. Onorato, *Physica D* **333**, 276 (2016).
  - [3] M. A. Hoefler, M. J. Ablowitz, I. Coddington, E. A. Cornell, P. Engels, and V. Schweikhard, *Phys. Rev. A* **74**, 023623 (2006).
  - [4] J. J. Chang, P. Engels, and M. A. Hoefler, *Phys. Rev. Lett.* **101**, 170404 (2008).
  - [5] W. Wan, S. Jia, and J. W. Fleischer, *Nat. Phys.* **3**, 46 (2007).
  - [6] C. Conti, A. Fratolocci, M. Peccianti, G. Ruocco, and S. Trillo, *Phys. Rev. Lett.* **102**, 083902 (2009).
  - [7] M. Marcianti and M. S. Murillo, *Phys. Rev. Lett.* **118**, 025001 (2017).
  - [8] V. E. Fortov, A. V. Ivlev, S. A. Khrapak, A. G. Khrapak, and G. E. Morfill, *Phys. Rep.* **421**, 1 (2005).
  - [9] G. E. Morfill and A. V. Ivlev, *Rev. Mod. Phys.* **81**, 1353 (2009).
  - [10] M. Bonitz, C. Henning, and D. Block, *Rep. Prog. Phys.* **73**, 066501 (2010).
  - [11] J. H. Chu and L. I, *Phys. Rev. Lett.* **72**, 4009 (1994).
  - [12] H. M. Thomas and G. E. Morfill, *Nature (London)* **379**, 806 (1996).
  - [13] A. Melzer, A. Homann, and A. Piel, *Phys. Rev. E* **53**, 2757 (1996).
  - [14] P. K. Shukla and A. A. Mamun, *Introduction to Dusty Plasma Physics* (Institute of Physics, Bristol, 2002).
  - [15] R. L. Merlino and J. A. Goree, *Phys. Today* **57(7)**, 32 (2004).
  - [16] A. Piel, *Plasma Physics* (Springer, Heidelberg, 2011), p. 2.
  - [17] A. Kananovich and J. Goree, *Phys. Rev. E* **101**, 043211 (2020).
  - [18] P. Hartmann, Z. Donkó, G. J. Kalman, S. Kyrkos, K. I. Golden, and M. Rosenberg, *Phys. Rev. Lett.* **103**, 245002 (2009).
  - [19] Y. Feng, J. Goree, and B. Liu, *Phys. Rev. Lett.* **100**, 205007 (2008).
  - [20] Y. Feng, J. Goree, and B. Liu, *Phys. Rev. Lett.* **104**, 165003 (2010).
  - [21] Y. Feng, J. Goree, and B. Liu, *Phys. Rev. Lett.* **109**, 185002 (2012).
  - [22] U. Konopka, G. E. Morfill, and L. Ratke, *Phys. Rev. Lett.* **84**, 891 (2000).
  - [23] A. Melzer, V. A. Schweigert, and A. Piel, *Phys. Rev. Lett.* **83**, 3194 (1999).
  - [24] A. V. Ivlev, M. H. Thoma, C. R ath, G. Joyce, and G. E. Morfill, *Phys. Rev. Lett.* **106**, 155001 (2011).
  - [25] Y. Feng, J. Goree, B. Liu, T. P. Intrator, and M. S. Murillo, *Phys. Rev. E* **90**, 013105 (2014).
  - [26] Y. Feng, J. Goree, and B. Liu, *Phys. Rev. Lett.* **105**, 025002 (2010).
  - [27] G. J. Kalman, P. Hartmann, Z. Donk o, and M. Rosenberg, *Phys. Rev. Lett.* **92**, 065001 (2004).
  - [28] P. Hartmann, M. Rosenberg, G. J. Kalman, and Z. Donk o, *Phys. Rev. E* **84**, 016409 (2011).
  - [29] K. Qiao, J. Kong, L. S. Matthews, and T. W. Hyde, *Phys. Rev. E* **91**, 053101 (2015).
  - [30] M. Bonitz, Z. Donk o, T. Ott, H. K ahlert, and P. Hartmann, *Phys. Rev. Lett.* **105**, 055002 (2010).
  - [31] A. Melzer, M. Klindworth, and A. Piel, *Phys. Rev. Lett.* **87**, 115002 (2001).
  - [32] P. Hartmann, A. Douglass, J. C. Reyes, L. S. Matthews, T. W. Hyde, A. Kov acs, and Z. Donk o, *Phys. Rev. Lett.* **105**, 115004 (2010).
  - [33] Y.-Y. Tsai, J.-Y. Tsai, and L. I, *Nat. Phys.* **12**, 573 (2016).
  - [34] C. Wong, J. Goree, Z. Haralson, and B. Liu, *Nat. Phys.* **14**, 21 (2018).
  - [35] Y.-f. He, B.-q. Ai, C.-x. Dai, C. Song, R.-q. Wang, W.-t. Sun, F.-c. Liu, and Y. Feng, *Phys. Rev. Lett.* **124**, 075001 (2020).
  - [36] P. Hartmann, Z. Donk o, T. Ott, H. K ahlert, and M. Bonitz, *Phys. Rev. Lett.* **111**, 155002 (2013).
  - [37] S. K. Sharma, A. Boruah, and H. Bailung, *Phys. Rev. E* **89**, 013110 (2014).

- [38] E. Thomas, Jr., R. Fisher, and R. L. Merlino, *Phys. Plasmas* **14**, 123701 (2007).
- [39] P. Harvey, C. Durniak, D. Samsonov, and G. Morfill, *Phys. Rev. E* **81**, 057401 (2010).
- [40] W. Lin, M. S. Murillo, and Y. Feng, *Phys. Rev. E* **100**, 043203 (2019).
- [41] Y. Rosenfeld, *Phys. Rev. E* **62**, 7524 (2000).
- [42] See <https://lammps.sandia.gov/>.
- [43] W. Lin, M. S. Murillo, and Y. Feng, *Phys. Rev. E* **101**, 013203 (2020).
- [44] K. Wang, D. Huang, and Y. Feng, *J. Phys. D* **51**, 245201 (2018).
- [45] Y. Feng, B. Liu, and J. Goree, *Phys. Rev. E* **78**, 026415 (2008).
- [46] See Supplemental Material at <http://link.aps.org/supplemental/10.1103/PhysRevE.103.013202> for our obtained time delay of shocks and the period of DSW for different conditions of 2D Yukawa systems, as well as the development of DSW from our simulations, which include Refs. [40,47,48].
- [47] P. Hartmann, G. J. Kalman, Z. Donkó, and K. Kutasi, *Phys. Rev. E* **72**, 026409 (2005).
- [48] W. Li, W. Lin, and Y. Feng, *Phys. Plasmas* **24**, 043702 (2017).